Study of Mechanisms of Light-Induced Dissociation of $Ru(dcbpy)(CO)_2I_2$ in Solution down to 20 fs Time Resolution

Viivi Lehtovuori,*,† Pasi Myllyperkiö,† Juha Linnanto,† Cristian Manzoni,‡ Dario Polli,‡ Giulio Cerullo,‡ Matti Haukka,§ and Jouko Korppi-Tommola†

Department of Chemistry Nanoscience Center, P.O. Box 35, FIN-40014, University of Jyväskylä, Finland, National Laboratory for Ultrafast and Ultraintense Optical Science−INFM-CNR Dipartimento di Fisica, Politecnico di Milano Piazza Leonardo da Vinci 32, I-20133 Milano, Italy, and University of Joensuu, Department of Chemistry, P.O. Box 111, FIN-80101 Joensuu, Finland

Received: November 18, 2004; In Final Form: July 19, 2005

Mechanisms of the light-induced ligand exchange reaction of (*trans*-I) $Ru(dcbpy)(CO)_2I_2$ (dcbpy = 4,4′-dicarboxylic acid-2,2′-bipyridine) in ethanol have been studied by transient absorption spectroscopy. Ultraviolet 20 fs excitation pulses centered at 325 nm were used to populate a vibrationally hot excited π^* bipyridyl state of the reactant that quickly relaxes to a dissociative Ru−I* state resulting in the release of one of the carbonyl groups. Quantum yield measurements have indicated that about 40% of the initially exited reactant molecules form the final photoproduct. A 62 fs rise component in the transient absorption (TA) signal was observed at all probe wavelengths in the visible region for the ongoing reaction, while the rise for the photoproduct was pulse limited (20 fs). We assign the observed 62 fs time component to the depopulation of the repulsive CO dissociative state. Vibrational coherences of the TA signals were observed at a wavenumber of 90 cm^{-1}. The resolved frequency, typical of I−Ru−I vibrational modes, is assigned to trans−cis isomerization of the iodines of the five-coordinated intermediate and damping of this oscillation in 500 fs to simultaneous solvent coordination. Cooling of the hot reactant and the product molecules occurs on a much slower time scale from 4 to 270 ps (Lehtovuori, V.; Aumanen, J.; Myllyperkiö, P.; Rini, M.; Nibbering, E. T. J.; Korppi-Tommola, J. *J. Phys. Chem. A* **2004**, *108,* 1644).

Introduction

Detailed study of reaction mechanisms of transition metal complexes, especially transition metal carbonyls, is of interest as they are used as catalysts in several important synthetic reactions.[1] Ultraviolet (UV) illumination of transition metal carbonyls often leads to dissociation of a CO group and thus to producing a reactive and short-lived coordinatively unsaturated intermediate species that may serve as a platform for further chemical reactions. Therefore, an understanding of the nature and dynamics of the reactive excited states as well as mechanisms of the formation of the intermediate species is of great importance.

In the gas phase, carbonyl dissociation is a very fast process taking place on the sub-100 fs time scale.[2−5] Dissociation of the first carbonyl group in the gas phase is often followed by a loss of one or more additional carbonyls, while in solution, only one carbonyl is lost under excitation.[6−8] In carbonyl complexes with α-diimine ligands (such as bipyridine), a charge transfer from mixed orbitals of the metal and the equatorial (cis to the diimine) CO ligands to the orbitals of axial (trans to the diimine) CO ligands takes place, giving rise to photochemical reactivity of these complexes.[9−11] It has been observed that the dissociation of equatorial CO results in a strong rearrangement of the remaining ligands around the metal center, while no such reorganization is seen after axial dissociation.[4,9,12,13] As the carbonyl group advances along the dissociation coordinate, one of the axial ligands moves toward the vacant equatorial site.[9] Such a mechanism would explain, for instance, formation of the CO back reaction product of *mer*-$MnCl(CO)_3$(α-diimine) after irradiation of the corresponding fac isomer.[14]

Upon UV excitation of transition metal carbonyl complexes, a greater amount of energy is deposited into the reacting molecule than is needed to dissociate the metal−CO bond. In the process, part of the excess energy is transformed into translational energy of the dissociating carbonyl group, and the rest is converted into heat via intramolecular vibrational redistribution, which finally is dissipated into the solvent. Excess kinetic energy allows the carbonyl group to escape the first solvation shell, a prerequisite for formation of the photoproduct. Correspondingly, the relative orientation of the CO ligand with respect to the molecules of the solvation shell at the time of excitation determines whether the released carbonyl will escape or whether the carbonyl will undergo back reaction to form the hot reactant. According to matrix isolation studies by Poliakoff and co-workers, the fate of the photoexcited, trapped species depends on the final orientation of the vacancy with respect to the surrounding atomic environment.[15] If the open position points toward a matrix atom, then it is likely that the five-coordinated intermediate will recombine to form the hot reactant. If the orientation is toward empty space in the matrix lattice, then CO is lost, and complexation of the five-coordinated intermediate and a lattice atom may take place. As the CO dissociation process is a very fast process (about 100 fs), similar orientation effects probably are present in solution, as solvent molecules in this time frame form a rigid matrix around the

* Corresponding author. E-mail: viivi.lehtovuori@cc.jyu.fi.
† University of Jyväskylä.
‡ National Laboratory for Ultrafast and Ultraintense Optical Science.
§ University of Joensuu.

10.1021/jp044735s CCC: $30.25
Published on Web 08/27/2005

solute. For several solution reactions, where the carbonyl had escaped the first solvation shell, it has been shown that the transition state complex reacts with a solvent molecule or a suitable nucleophile to form the final photoproduct.[16−21] Solvent coordination takes place within a few picoseconds or less.[16,18−20] Typically, in solution the quantum yields of photoinduced reactions of the metal carbonyls are significantly less than unity.[12,17] The relative efficiencies of the initial excitation, internal conversion after excitation, and CO recombination reaction finally determine the total quantum yield of the reaction.[7,8,19,22−27]

According to crystal structure determination the complex in the present study, (*trans*-I)Ru(dcbpy)$(CO)_2I_2$ (dcbpy = 4,4′-dicarboxy-2,2′-bipyridine) has two equatorial CO groups and two axial halogens.[13] Structural, infrared, and NMR spectroscopic evidence for the photoproduct suggests that under illumination, the reactant loses one of its CO groups and the axial halogens change orientation from trans to cis.[12,28] One may expect the CO dissociation to be a relatively fast process, followed by a slower trans−cis isomerization of the heavier iodine ligands. An axial site then would be left open for solvent binding. The photoreaction dynamics of (*trans*-I)Ru(dcbpy)-$(CO)_2I_2$ have been previously studied by transient UV-pump/IR-probe spectroscopy with a time resolution of ∼170 fs.[29] From the infrared experiments, it became evident that both the reactant and the photoproduct remained vibrationally hot in the solution for quite a long time, as the red shifted CO stretching bands of the reactant decayed in 4 and 80 ps and the initially broad product (transition state complex) absorption band was narrowed to its final shape in 18 and 270 ps.

In our previous femtosecond transient experiments in the visible[30] and IR regions,[29] we were not able to resolve the fast initial steps of the reaction. In this work, to study the early events of the photoreaction, we used excitation pulses of ∼20 fs duration centered at 325 nm and sub-10 fs probe pulses (500−700 nm) thus obtaining a temporal resolution of ∼20 fs over most of the visible spectral region. The main objective of the study was to try to observe the processes of carbonyl dissociation, formation of the transition state complex, trans−cis isomerization of the halogens, and solvent attachment to the transition state complex in real time. To aid the interpretation of the kinetic data, we used quantum chemical calculations to evaluate the electronic and vibrational transition energies of the reactant, the five-coordinated intermediate, and the photoproduct.

Experimental Procedures

Steady-State Spectroscopy. Synthesis and characterization of the reactant complex are described elsewhere.[12] The photoproduct was prepared by illuminating the sample with visible (λ < 500 nm) or UV light, and the advancement of the reaction was followed by recording the steady-state UV (Varian Cary 100) or IR spectra (Nicolet Magna 760 FTIR). For quantum yield measurements, the excitation bandwidth from a Xe-lamp (300 W, Oriel 6259) was selected with interference filters ($\Delta\lambda$ ∼5−6 nm), and advancement of the reaction was monitored at 600 nm.

Transient Absorption Measurements. To replenish the sample between consecutive laser pulses in the transient absorption measurements, an ethanol solution of the sample was flowed by a peristaltic pump through a cell equipped with a 100 μm thick front window made of quartz. The optical density of the sample at the excitation wavelength (325 nm) was ∼1 in a 1 mm cuvette. Overlap of the pump and the probe beams (interaction length 200−300 μm) was placed close to the front window of the cuvette to minimize the group velocity mismatch between the pump and the probe beams. The femtosecond setup consisted of an amplified Ti:sapphire laser, generating 150 fs, 500 μJ pulses at 780 nm and a 1 kHz repetition rate. The fundamental beam was used to pump two noncollinear visible optical parametric amplifiers (NOPAs).[31] The first NOPA (NOPA1) generated pulses with 20−30 THz bandwidth, tunable from 500 to 700 nm, which were compressed to nearly the transform-limited 15−20 fs duration by multiple reflections on chirped mirrors. The second NOPA (NOPA2) generated ultra broadband pulses spanning the 500−700 nm wavelength range and compressed to sub-10 fs duration also by multiple reflections on chirped mirrors.[32] Pulses from NOPA1 were frequency up-converted to the UV by sum-frequency generation with the fundamental 780 nm light in a 50 μm thick BBO crystal. A type II phase matching configuration was used to provide the necessary up-conversion bandwidth. The UV pulses were then compressed to a 20−25 fs duration by a double pass in a pair of fused silica prisms.

The pulses from NOPA1 and NOPA2 were synchronized by a delay line and focused on the sample using only reflective optics in a standard noncollinear pump−probe configuration. The pump pulse energy at the sample was approximately 25 nJ. Time-resolved measurements at specific wavelengths were obtained by spectral filtering (10 nm bandwidth) the probe beam after passing through the sample and combining differential detection with lock-in amplification. In all measurements, the maximum $\Delta T/T$ signal was less than 6%, ensuring that saturation was not occurring. The instrument response function was determined by measuring the $\Delta T/T$ signal of a C_{60} film, showing an instantaneously rising transient absorption signal.[33] Signals of the pure solvent were also measured. Ethanol has only minor absorption at the excitation wavelength; therefore, signals arising from pure solvent were small, with a derivative-like shape characteristic of cross-phase modulation, and their contribution to the signal arising from the sample was negligible.

Calculations. The full geometry optimizations of all structures, the reactant, the five-coordinated intermediate, and the product were carried out by using the nonlocal hybrid density functional method B3PW91, as implemented in the Gaussian98 program.[34] The basis set was the standard 6-31G* for all elements except Ru and I, for which the Huzinaga's bases 433321/4331/421 and 433321/43321/431 were used.[34] The basis sets were augmented by the polarization function of p-type with an exponent of 0.086 for Ru and function of d-type with an exponent of 0.266.[35] The Hessian matrix was calculated analytically for all structures to prove the location of correct minima (none of the structures had imaginary frequencies). The thermodynamic energies have been calculated at 298.15 K. Calculations were performed on COMPAQ ES40 four processor workstations and on personal computers.

Excited-state energies and oscillator strengths of the B3PW91/6-31G* optimized structures were calculated by using the ZINDO/S CIS configuration interaction method with 45 occupied and 45 unoccupied molecular orbitals and the dipole velocity approach.[36−39] To account for the inhomogeneous broadening of the spectral lines, the stick spectra were convoluted with a Gaussian distribution of transition energies. The fwhm (full width half-maximum) of the Gaussian distribution was set to be 1500 cm^{-1} in the spectral range studied. No scaling of the calculated energies was made.

Results

Spectroscopic Signatures of the Reaction. Figure 1A shows the calculated excited-state energy levels of the reactant and

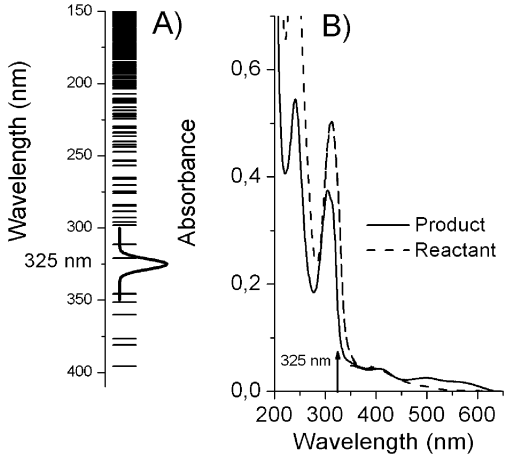

Figure 1. (A) Calculated excited-state energy levels of the reactant (ZINDO/S CIS (45,45)) and the Gaussian excitation pulse centered at 325 nm. (B) UV−vis absorption solution spectra of the reactant (dashed line) and the product (solid line), respectively.

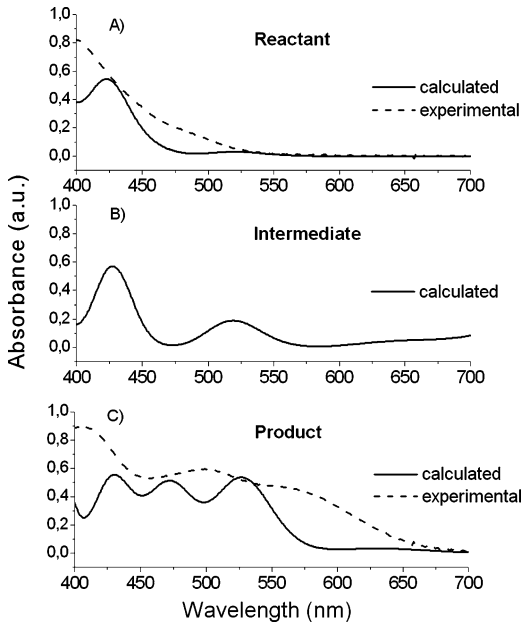

Figure 2. Calculated (solid) and experimental (dashed) ground-state absorption spectra of (A) the reactant, (B) the five-coordinated intermediate, and (C) the photoproduct in the visible spectral region.

the spectrum of the 20 fs excitation pulse centered at 325 nm. The experimental absorption spectrum of the reactant shows intense UV absorption bands at 250 nm and at 320 nm and a broad and weak absorption band centered at 400 nm (dashed line in Figure 1B). Beyond 520 nm, there is practically no ground-state absorption of the reactant (see Figure 1B); however, both our ZINDO calculations and our earlier transient absorption measurements show broad excited-state absorption (ESA) of the reactant with a maximum around 500 nm.[30] Under UV or visible illumination, a broad ground-state absorption band characteristic of the photoproduct, extending from 500 to 650 nm, appears in the spectrum (Figure 2). Advancement of the reaction is also visible in the infrared spectrum: under illumination, the two CO stretching bands of the reactant, the symmetric at 2002 cm^{-1} and the antisymmetric at 2058 cm^{-1}, disappear, and concurrently, a well-separated singlet absorption at 1970 cm^{-1} is formed, a clear indication of a loss of one of the equatorial CO groups in the photo process. As described previously, the reactant has two axial iodine ligands and two equatorial carbonyl ligands.[13] The crystal structure of the

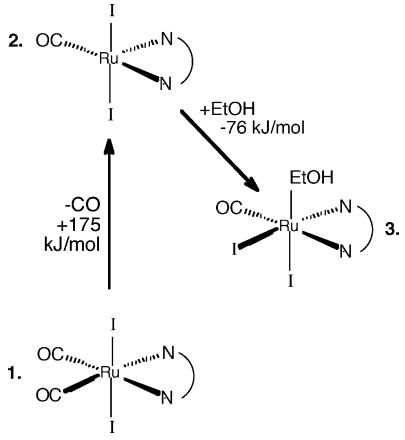

Figure 3. Schematic structures of the reactant (**1**) and the photoproduct (**3**) inferred from the experimental results shown with the hypothetical structure of the reaction intermediate (**2**). Energies given refer to calculated thermodynamic energy differences of the minimum energy DFT structures of **2** and **3** with respect to **1**.

photoproduct is not known. However, the crystal structure of the photoproduct of a very similar complex (*trans*-Cl)Ru(bpy)-$(CO)_2Cl_2$ reveals that a solvent molecule (i.e., CH_3CN or alcohol) occupies an axial position and that the halogens are in a cis orientation.[28] Comparison of proton magnetic resonance spectra in the aromatic (bpy protons) region of (*cis*-Cl)Ru(bpy)-(Sol)(CO)Cl_2 and the photoproduct of (*trans*-I)Ru(dcbpy)$(CO)_2I_2$ provides strong evidence for similarity of the two structures. Also, density functional calculations for the photoproduct give a minimum for such ligand coordination. It is then most probable that the photoproduct of the present complex has a solvent molecule in an axial position, that the two iodines are in a cis orientation, and that the photoproduct may be characterized as (*cis*-I)Ru(dcbpy)(CO)$(CH_3CH_2OH)I_2$[12] (Figure 3).

The quantum yield of the photoreaction has been previously determined to be 0.3 (with 458 nm excitation), indicating that only one-third of the excited molecules undergoes reaction to form product molecules.[12] Further quantum yield measurements were carried out by using tunable excitation, indicating an increase of the quantum yield from 0.3 to 0.4 upon changing the excitation wavelength from 458 to 311 nm.

Simulation of Spectra. The minimum energy density functional theory (DFT) geometry of the reactant was in good agreement with the experimental crystal structure. Minimum energy DFT geometries of the photoproduct and the five-coordinated intermediate were also found. The calculated frequencies of CO symmetric and asymmetric stretching modes (not scaled) of the reactant are 2116 cm^{-1} (exp. 2002 cm^{-1}) and 2159 cm^{-1} (exp. 2058 cm^{-1}), respectively, about 100 cm^{-1} higher than the experimental values, which is a typical result for systems of this size. The difference, however, between the two experimental frequencies was well-predicted. For the photoproduct, the calculated CO stretching frequency was 2087 cm^{-1} (exp. 1962 cm^{-1}). The calculated CO stretching frequency of the five-coordinated intermediate was 2113 cm^{-1}, clearly higher than that of the photoproduct. Calculations provided a basis for assignments of the I−Ru−I vibrational modes of the five-coordinated intermediate that were resolved in the transient absorption signals of the ongoing reaction.

The ZINDO/CI method was used to estimate the electronic absorption spectra of the reactant, the product, and the five-coordinated intermediate. According to calculations, the oscillator strength of the reactant was very low for wavelengths longer than 475 nm, while the photoproduct shows a broad

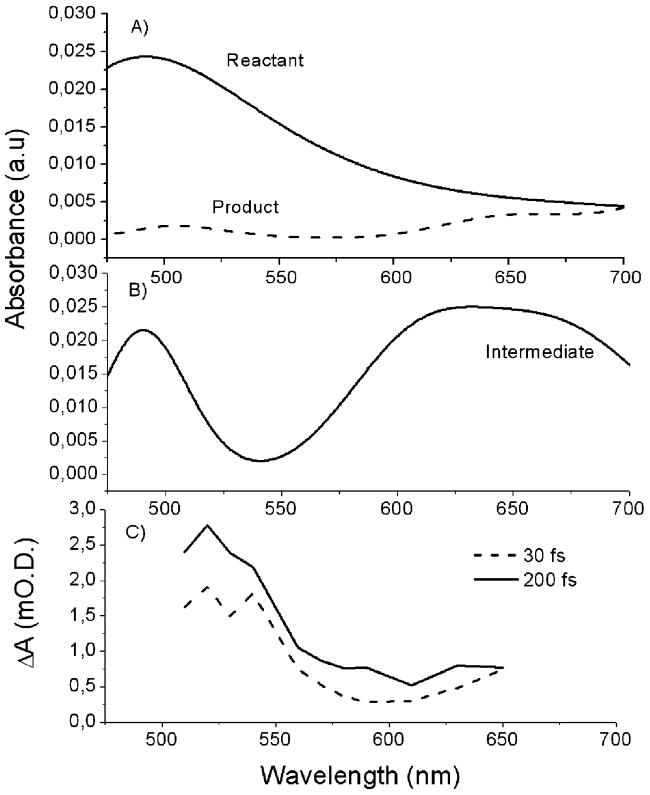

Figure 4. Calculated excited-state spectra of (A) the reactant (solid line) and the product (dashed line) and (B) the five-coordinated intermediate. Panel C shows approximate transient spectrum of the ongoing reaction at time delays of 30 fs (dashed line) and 200 fs (solid line) after excitation.

absorption from 475 to 625 nm, in accordance with the experimental spectra (Figure 2). Calculations also predicted that the five-coordinated intermediate has a much stronger absorption from 500 to 550 nm than the reactant (Figure 2B). The experimental transient absorption spectra of the studied complexes was comprised mostly of absorption of the excited states. Therefore, the excited state absorption spectra were also calculated (see Figure 4). Since the calculated excited state absorption spectra did not include excited state emissions or any other relaxation processes, the calculated ESA spectra yielded a qualitative picture of transient spectra of the molecules immediately after excitation. According to these results, the ESA spectrum of the reactant shows a maximum around 500 nm, whereas the five-coordinated intermediate has two excited-state absorption maxima: one around 500 nm and a broad red-shifted absorption around 640 nm. The ESA of the photoproduct at 500 nm was much weaker than that of either the reactant or the five-coordinated intermediate. The most intense excited-state absorption of the three was that of the photoproduct around 800 nm (not shown in Figure 4).

Transient Absorption Measurements. Following excitation by a 20 fs pulse centered at 325 nm, transient absorption (TA) signals of the ongoing reaction showed increased absorption with almost identical dynamics at probe wavelengths from 510 to 650 nm (Figure 5). At all wavelengths probed, approximately 50% of the rise of the signal occurs within the pulse, and the rest of the signal rises exponentially with a rise time of 62 ± 5 fs. At longer time delays (picosecond time scale), the transient absorption signal shows exponential decay components of 4, 70, 18, and 270 ps. The same constants were observed in the mid-infrared femtosecond experiments for the reactant and photoproduct (see Figure 7 of ref 29).[29] In the visible region, it

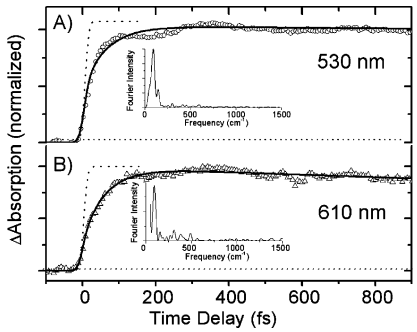

Figure 5. Rise of the signal (A) at 530 nm and (B) at 610 nm. At both wavelengths, the data have been fitted with one rise component of 62 fs. The Fourier spectrum of the data is shown in the inset. Dotted lines denote the integrated instrument response function.

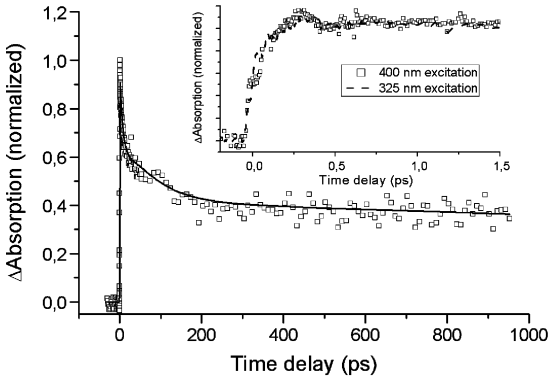

Figure 6. Kinetics of the reaction at 570 nm at time delays up to 1 ns after 200 fs excitation centered at 400 nm. Open squares are the data points and a four component exponential fit as the solid line with rise times of 4.3 (21%) ps, 18 (17%) ps, 70 (19%) ps, and 270 (5%) ps. Observe that the signal remains positive at delays longer than 1 ns (38%), an indication of the formation of the photoproduct absorbing in this wavelength region. The inset shows TA signals after 400 nm (open squares) and 325 nm (dashed line) excitations at the probe wavelength 570 nm at early time delays.

was not possible to distinguish the contributions of the reactant and the photoproduct to these decays.

The lowest panel of Figure 4 shows the experimental TA spectra of the reacting system at time delays of 30 and 200 fs after 325 nm excitation. The calculated ESA spectra suggest that the experimental transient spectra from 520 to about 550 nm contain a contribution mainly from the reactant and the five-coordinated intermediate and only a minor contribution from the photoproduct. From 550 nm toward red, absorption of the intermediate becomes dominant. The calculations, however, give only a qualitative picture of the excited state absorptions, and the relative absorption coefficients of various transitions in the experimental spectra ultimately determine the shape and evolution of the transient spectra.

Coherent oscillations were present in all recorded kinetic signals (Figure 5). A Fourier transform analysis assigns the frequency of oscillation, which is present at all probe wavelengths, at 90 ± 5 cm^{-1}. Exponential damping of this oscillation was fitted with a rise time of 500 ± 30 fs. To check the effect of excitation wavelength on the kinetics, the experiments were repeated by using 400 nm excitation. Time resolution in this measurement was ~90 fs. As can be seen from Figure 6, at time delays longer than 100 fs, the signals behave identically, showing low-frequency oscillations and similar decay components.

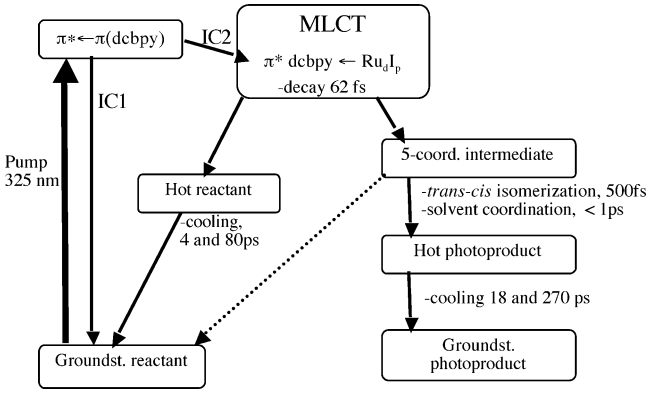

Figure 7. Schematic presentation of various phases of the photoreaction.

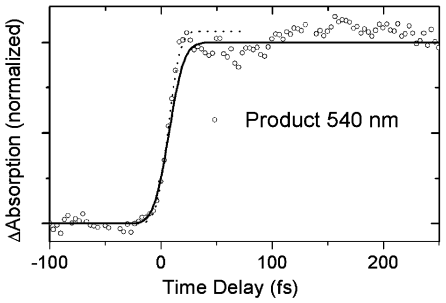

Figure 8. ESA kinetics of the photoproduct molecule after 320 nm excitation. The signal rises within the excitation pulse in contrast to the solution undergoing the reaction, which has a rise time of 62 fs. The signal-to-noise ratio is reduced by the weaker absorption of the $\pi^* \leftarrow \pi$ dcbpy transition in the product molecules at the pump wavelength; see Figure 1.

Discussion

The purpose of our study was to understand of the mechanisms of the CO dissociation and the consequent reactions. In addition, an explanation was sought for the observed low quantum yield of ~0.4 of the reaction. Both the calculated ground state absorption and the excited state absorption spectra of the reactant correspond reasonably well with the experiments, which lent confidence to the calculated excited-state transitions. A possible sequence of various phases of the studied photoreaction is shown in Figure 7. According to the ZINDO/S CI calculations, the 325 nm excitation transfers an electron from the bonding π orbital of the dcbpy ligand to the antibonding π^* orbital (Figure 1) of the same ligand. After excitation, several relaxation pathways are possible: internal conversion (IC) to the ground state or to a lower energy excited state (IC1 in Figure 7), intersystem crossing (ISC) to a triplet state, and predissociation (IC2 in Figure 7). It is unlikely that the initially excited state, which is entirely localized to the dcbpy ligand, leads to CO dissociation. To make charge redistribution of a Ru−CO bond (weakening of the bond) possible, an IC to a dissociative potential surface has to take place. As a potential candidate for such a repulsive state, we consider the MLCT state, involving charge transfer from the mixed Ru−I orbitals lying energetically below the initially excited state.[30] As a result of the crossover to the dissociative state, a carbonyl group will be detached. Such a carbonyl group contains a substantial amount of kinetic energy. Two possibilities exist for the fragment propagation: either the CO ligand escapes the first solvation shell or it undergoes geminate recombination. In the first case, it is highly unlikely that the CO ligand finds its way back to the original binding site (dashed arrow in the Figure 7). Followed by dissociation, an intermediate is formed, and it may react, during its characteristic lifetime, with one of the nearest solvent molecules to form the final photoproduct. If the energetic CO group collides with a solvent molecule, it probably rebounds to reform a hot reactant molecule.

Consider that the initially excited π^* state is a bound state of the bpy ligand. Approximately 50% of the TA signal is pulse limited, probably due to ESA from this state. We suggest that the observed rise time of 62 fs is related to the decay of population of the dissociative state, namely, to the MLCT state. The dissociative potential is in effect a bound state since the surrounding solvent molecules generate a diverse potential around the reacting molecule depending on the relative position and orientation of the solvent molecules. Only a fraction of the population of the dissociative state undergoes dissociation, where the CO group escapes from the solvent cage resulting in formation of the five-coordinated intermediate. The rest of the population either rebounds from the solvation shell or decays to lower energy excited states of the reactant. This process might be considered as geminate recombination or avoided dissociation. In general, one would expect to observe the depopulation of a dissociative state as a decay in the transient absorption signal. However, we observe these processes as a rise of an ESA signal since this signal does not arise from absorption from the dissociative surface but rather absorption from excited states of the intermediate and the hot reactant molecule. Since we are not able to determine the efficiency of the internal conversion of the initially excited state to the dissociative state (IC2 on Figure 7) and the relative proportion of geminate recombination, we cannot determine time constants for these individual processes. However, we can estimate the time frame for the dissociation: the upper limit of 170 fs is obtained from the previous transient IR experiment, and the lower limit of 62 fs is valid if the observed quantum yield is purely due to competition between IC1 and IC2 without any geminate recombination. A convincing proof for the assignment of the observed rise time to the photodissociation reaction was obtained by repeating the measurement under conditions where the reactant molecules were completely transformed into photoproducts in the excitation volume. The ESA signal for the photoproduct is shown in Figure 8. Only an instantaneous rise was observed, confirming that the 62 fs rise time is related to CO dissociation and formation of the five-coordinated intermediate. The observed rise of the signal of the photoproduct shown in Figure 8 also demonstrates that no significant pulse broadening due to the cell front window or in the interaction length of the two laser beams has taken place.

In principle, the 62 fs rise time could be due to ISC to a triplet state. Extremely fast sub-100 fs ISC processes competing with parallel ultrafast processes have been reported for several ruthenium bipyridyls.[40−42] At 77 K, the reactant shows a long-lived triplet emission with a large Stokes shift.[12,30] Emission is almost completely quenched at 130 K, and it is not observable at room temperature. Emission from the photoproduct at 77 K is much weaker than that of the reactant.[30] At room temperature, practically no emission from the reactant or the photoproduct has been seen. The transient IR spectrum of the ongoing reaction in the CO stretching region recovers in less than 300 ps at room temperature. As triplet states normally live much longer, it is likely that triplet states are not populated during the present photoreaction.

At all probe wavelengths, a low-frequency oscillation (90 cm^{-1}, 370 fs period) damped in 500 ± 30 fs was observed. The damping was much slower than the rise of the signal. This coherence, due to its longer lifetime, is assigned to the five-

coordinated intermediate. The 90 cm^{-1} frequency was also resolved after direct excitation of the π^*(dcbpy) ← Ru_dI_p transition at 400 nm with 90 fs pulses, which indicates that the oscillation is not dependent on the initially prepared state (see Figure 6). A total oscillation time of about ~1 ps indicates that coherence survives dissociation and is transferred from the optically prepared state of the reactant to vibrational modes of the five-coordinated intermediate. Other examples of vibrationally coherent photochemistry have been previously reported in several systems.[43−46] Comparison of the structures of the reactant and the photoproduct suggests that after dissociation, the five-coordinated intermediate undergoes a conformational change, where an iodine ligand changes its orientation from trans to cis relative to the dcbpy nitrogens.[12] As a first guess, the modes responsible for such a conformational change are those related to I−Ru−I bending and/or stretching vibrations. The DFT ground-state frequencies of the I−Ru−I stretching and bending modes of the five-coordinated intermediate are at 138 and 41 cm^{-1}, respectively. These numbers should be considered as an order of magnitude estimates, as trans to cis isomerization is a large amplitude motion. However, their mean is very close to the observed value of 90 cm^{-1}. Alternatively, as the shapes of the potential energy surfaces of the reactant molecule are unknown, we cannot exclude the possibility that the oscillations would arise from electronic ground-state wave packet generated from a stimulated Raman process within the pump pulse. The results do not give a clear answer as to whether the dissociation is taking place in the excited state or in the ground state. Excitation to higher electronic states is needed to initiate the reaction that is to break the Ru−CO bond (calculated dissociation energy 175 kJ/mol). For several flexible molecules, light-induced conformational changes have been observed in the excited state.[47−49] In the present case, trans−cis isomerization must have a low barrier since the photoproduct is obtained in the pure cis form. This, in fact, supports the assumption that the trans−cis isomerization of the five-coordinated intermediate takes place in the excited state where barriers, in general, are much lower than those in the ground state.

If the oscillations were due to conformational changes, then the damping of the oscillation could describe the ceasing of the bending motion of the iodine as the solvent molecule occupies the vacant axial site. We have also measured the excited state decays of the ongoing reaction in several *n*-alcohols with ~150 fs time resolution at several wavelengths in the visible spectral region.[29] At time delays longer than 1 ps, the TA signals were to be independent of solvent. This result suggests that solvent attachment takes place roughly on the same time scale as the conformational change of the iodine atoms. It was pointed out that cooling of the hot reactant and the photoproduct occurs in the much longer time window of 4 ps $< \tau <$ 270 ps.[29]

Conclusions

We have measured the femtosecond dynamics of the light-induced ligand exchange reaction of $Ru(dcbpy)(CO)_2I_2$ with 20 fs time resolution. The results together with quantum chemical calculations support the interpretation that the initially excited π^* state of the dcpby ligand depopulates via a very fast internal conversion to a repulsive potential energy surface and possibly partly to a lower lying excited bound state. After this initial step, the CO ligand proceeds along the reaction coordinate to form the five-coordinated intermediate. The CO ligand on the repulsive potential surface has large translational energy, and it either rebounds the nearest solvent molecule to form the hot reactant (geminate recombination) or it may escape beyond the first solvation shell (dissociation). Our previous femtosecond infrared results and the quantum yield measurements suggest that ~40% of the initially excited complexes form the final photoproduct. We assign the observed rise of the transient absorption signal of 62 fs to the carbonyl dissociation and relaxation to the lower energy levels of the hot recombined reactant. The coherent low-frequency oscillation of 90 cm^{-1} observed with all visible probe wavelengths and for two different pump wavelengths is indicative of a trans−cis isomerization of the iodines of the five-coordinated intermediate. Exponential damping of this oscillation in 500 fs was assigned to solvent attachment to an open axial site. The transient absorption kinetics of the complex in several alcohol solutions did not show solvent dependence for time delays longer than 1 ps, which is considered an upper time limit of solvent coordination.

Acknowledgment. V.L. and J.K.-T. acknowledge support form the European Community−Access to Research Infrastructure Action of the Improving Human Potential Program, Contract HPRI-CT-2001-00148 (Center for Ultrafast Science and Biomedical Optics). Financial support from the Academy of the Finland (Contract 50670) is also acknowledged.

References and Notes

(1) Kalyanasundaram, K.; Grätzel, M., Eds. *Photosensitization and Photocatalysis Using Inorganic and Organometallic Compounds*; Kluwer Academic Publishers: Dordrecht, The Netherlands, 1993.

(2) Kim, S.; Pedersen, S.; Zewail, A. H. *Chem. Phys. Lett*. **1995**, *233*, 500.

(3) Trushin, S.; Fuss, W.; Schmid, W.; Kompa, K. *J. Phys. Chem. A* **1998**, *102*, 4129.

(4) Paterson, M.; Hunt, P.; Robb, M.; Takahashi, O. *J. Phys. Chem. A* **2002**, *106*, 10494.

(5) Chantal, D.; Full, J.; Gonzàles, L.; Kaposta, K.; Krenz, M.; Lupulescu, C.; Manz, J.; Minemoto, S.; Oppel, M.; Rosendo-Francisco, P.; Vajda, S.; Wöste, L. *Chem. Phys.* **2001**, *267*, 247.

(6) Vlcek, A., Jr.; Farrel, I. R.; Liard, D. J.; Matousek, P.; Towrie, M.; Parker, A. W.; Grills, D. C.; George, M. W. *J. Chem. Soc., Dalton Trans.* **2002**, 701.

(7) Guillamont, D.; Vlcek, A., Jr.; Daniel, C. *J. Phys. Chem. A* **2001**, *105*, 1107.

(8) Yang, H.; Snee, P.; Kotz, K.; Payne, C.; Harris, C. B. *J. Am. Chem. Soc*. **2001**, *123*, 4204.

(9) Rosa, A.; Riccardi, G.; Baerends, J. E.; Stufkens, D. J. *J. Phys. Chem. A* **1996**, *100*, 15346.

(10) Goumans, T. P. M.; Ehlers, A. W.; van Hemert, M. C.; Rosa, A.; Baerends, E.-J.; Lammertsma, K. *J. Am. Chem. Soc.* **2003**, *125*, 3558.

(11) Zalis, S.; Farrel, I. R.; Vlcek, A., Jr. *J. Am. Chem. Soc*. **2003**, *125*, 4580.

(12) Luukkanen, S.; Haukka, M.; Eskelinen, E.; Pakkanen, T. A.; Lehtovuori, V.; Kallioinen, J.; Myllyperkiö, P.; Korppi-Tommola, J. *Phys. Chem. Chem. Phys*. **2001**, *3*, 1992.

(13) Trushin, S. A.; Fuss, W.; Schmid, W. E. *Chem. Phys*. **2000**, *259*, 313.

(14) Stor, G. J.; Morrison, S. L.; Stufkens, D. J.; Oskam, A. *Organometallics* **1994**, *13*, 2641.

(15) Turner, J. J.; Burdett, J. K.; Perutz, R. N.; Poliakoff, M. *Pure Appl. Chem*. **1979**, *49*, 271.

(16) Joly, A.; Nelson, K. *J. Phys. Chem*. **1989**, *93*, 2876.

(17) Simon, J.; Xie, X. *J. Phys. Chem*. **1986**, *90*, 6751.

(18) O'Driscoll, E.; Simon, J. *J. Am. Chem. Soc.* **1990**, *112*, 6580.

(19) Bromberg, S.; Lian, T.; Bergman, R.; Harris, C. B. *J. Am. Chem. Soc*. **1996**, *118*, 2069.

(20) Dougherty, T.; Heilweil, E. *Chem. Phys. Lett*. **1994**, *227*, 19.

(21) Owrutsky, J.; Baronavski, A. *J. Chem. Phys*. **1996**, *105*, 9864.

(22) Lian, T.; Bromberg, S. E.; Asplund, M. C.; Yang, H.; Harris, C. B. *J. Phys. Chem. A* **1996**, *100*, 11994.

(23) Vlcek, A., Jr. *Coord. Chem. Rev.* **2002**, *230*, 225.

(24) Farrel, I. R.; Matousek, P.; Towrie, M.; Parker, A. W.; Vlcek, A., Jr. *Inorg. Chem*. **2002**, *17*, 4318.

(25) Vichová, J.; Hartl, F.; Vlcek, A., Jr. *J. Am. Chem. Soc.* **1992**, *114*, 10903.

(26) Rini, M.; Holm, A.-K.; Nibbering, E. T. J.; Fidder, H. *J. Am. Chem. Soc*. **2002**, *128*, 3028.

(27) Vlcek, A., Jr.; Farrel, I. R.; Liard, D. J.; Matousek, P.; Towrie, M.; Parker, A. W.; Grills, D. C.; George, M. W. *J. Chem. Soc., Dalton Trans.* **2002**, 701.

(28) Eskelinen, E.; Haukka, M.; Venäläinen, T.; Pakkanen, T.; Wasberg, M.; Chardon-Noblat, S.; Deronzier, A. *Organometallics* **2000**, *19*, 163.

(29) Lehtovuori, V.; Aumanen, J.; Myllyperkiö, P.; Rini, M.; Nibbering, E. T. J.; Korppi-Tommola, J. *J. Phys. Chem. A* **2004**, *108*, 1644.

(30) Lehtovuori, V.; Kallioinen, J.; Myllyperkiö, P.; Haukka, M.; Korppi-Tommola, J. *Chem. Phys*. **2003**, *295*, 81.

(31) Cerullo, G.; Nisoli, M.; De Silvestri, S. *Appl. Phys. Lett.* **1997**, *71*, 3616.

(32) Zavelani-Rossi, M.; Cerullo, G.; De Silvestri, S.; Gallmann, L.; Matuschek, N.; Steinmeyer, G.; Keller, U.; Angelow, G.; Scheuer, V.; Tschudi, T. *Opt. Lett.* **2001**, *26*, 1155.

(33) Dexheimer, S. L.; Vareka, W. A.; Mittleman, D.; Zettl, A.; Shank, C. V. *Chem. Phys. Lett.* **1995**, *235*, 552.

(34) Frisch, M. J.; Trucks, G. W.; Schlegel, H. B.; Scuseria, G. E.; Robb, M. A.; Cheeseman, J. R.; Zakrzewski, V. G.; Montgomery, J. A., Jr.; Stratmann, R. E.; Burant, J. C.; Dapprich, S.; Millam, J. M.; Daniels, A. D.; Kudin, K. N.; Strain, M. C.; Farkas, O.; Tomasi, J.; Barone, V.; Cossi, M.; Cammi, R.; Mennucci, B.; Pomelli, C.; Adamo, C.; Clifford, S.; Ochterski, J.; Petersson, G. A.; Ayala, P. Y.; Cui, Q.; Morokuma, K.; Malick, D. K.; Rabuck, A. D.; Raghavachari, K.; Foresman, J. B.; Cioslowski, J.; Ortiz, J. V.; Stefanov, B. B.; Liu, G.; Liashenko, A.; Piskorz, P.; Komaromi, I.; Gomperts, R.; Martin, R. L.; Fox, D. J.; Keith, T.; Al-Laham, M. A.; Peng, C. Y.; Nanayakkara, A.; Gonzalez, C.; Challacombe, M.; Gill, P. M. W.; Johnson, B. G.; Chen, W.; Wong, M. W.; Andres, J. L.; Head-Gordon, M.; Replogle, E. S.; Pople, J. A. *Gaussian 98*; Gaussian, Inc.: Pittsburgh, PA, 1998.

(35) Huzinaga, S., Ed. *Gaussian Basis Sets for Molecular Calculations; Physical Sciences Data 16*; Elsevier: Amsterdam, 1984.

(36) Karlsson, G.; Zerner, M. C. *Int. J. Quantum Chem*. **1977**, *3*, 35.

(37) Ridley, J.; Zerner, M. *Theor. Chim. Acta* **1973**, *32*, 111.

(38) Ridley, J. E.; Zerner, M. C. *Theor. Chim. Acta* **1976**, *42*, 223.

(39) Zerner, M. C.; Loew, G. H.; Kirchner, R. F.; Mueller-Westerhoff, U. T. *J. Am. Chem. Soc*. **1980**, *102*, 589.

(40) Damraurer, N. H.; Cerullo, G.; Yeh, A.; Boussie, T. R.; Shank, C. H.; McCusker, J. K. *Science* **1997**, *257*, 54.

(41) Kallioinen, J.; Benkö, G.; Yartsev, A.; Korppi-Tommola, J. E. I.; Sundström, V. *J. Phys. Chem. B* **2002**, *106*, 4396.

(42) Benkö, G.; Kallioinen, J.; Korppi-Tommola, J. E. I.; Yartsev, A.; Sundström, V. *J. Am. Chem. Soc*. **2002**, *124*, 498.

(43) Wang, Q.; Peteanu, L.; Schoenlein, R. W.; Shank, C. V.; Mathies, R. *Science* **1994**, *266*, 422.

(44) Zhu, L.; Sage, J. T.; Champion, P. M. *Science* **1994**, *266*, 629.

(45) Vos, M. H.; Rappaport, F.; Lambry, J. C.; Breton, J.; Martin, J. L. *Nature* **1993**, *363*, 320.

(46) Wurzer, A. J.; Lochbrunner, S.; Riedle, E. *Appl. Phys. B* **2000**, *71*, 405.

(47) Schultz, T.; Quenneville, J.; Levine, B.; Toniolo, A.; Martinez, T. J.; Lochbrunner, S.; Schmitt, M.; Shaffer, J. P.; Zgierski, M. Z.; Stolow, A. *J. Am. Chem. Soc*. **2003**, *125*, 8098.

(48) Fujino, T.; Arzhantsev, S. Yu.; Tahara, T. *J. Phys. Chem. A* **2001**, *105*, 8123.

(49) Bussotti, L.; Cacelli, I.; D'Auria, M.; Foggi, P.; Lesma, G.; Silvani, A.; Villani, V. *J. Phys. Chem. A* **2003**, *107*, 9079.